



Full Text View

[Volume 30, Issue 8 \(August 2000\)](#)

Journal of Physical Oceanography

Article: pp. 1931–1943 | [Abstract](#) | [PDF \(226K\)](#)

Wave Crest Distributions: Observations and Second-Order Theory

George Z. Forristall

Shell E&P Technology, Houston, Texas

(Manuscript received February 2, 1999, in final form September 14, 1999)

DOI: 10.1175/1520-0485(2000)030<1931:WCDOAS>2.0.CO;2

ABSTRACT

Many empirical and heuristic distribution functions for wave crest heights have been proposed, but their predictions differ considerably. Part of the lack of agreement is due to the difficulty of making measurements that accurately record the true height of the wave crests. Surface following buoys effectively cancel out the second-order nonlinearity by making a Lagrangian measurement. Pressure transducers filter the nonlinear components of the signal in complicated ways. Wave staffs have varying degrees of sensitivity to spray. The location of the instruments also plays an important role. There is clear evidence from measurements in the North Sea that spurious crests due to spray are a problem downwind even from mounting supports that appear transparent.

Much of the theoretical nonlinearity can be captured by calculations correct to second order. Explicit calculation of the interactions of each pair of components in a directional spectrum is straightforward although computationally intensive. This technique has the advantage that the effects of wave steepness, water depth, and directional spreading are included with no approximation other than the truncation of the expansion at second order. Comparisons with measurements that are believed to be of the best quality show good agreement with these second-order calculations. Simulations for a set of JONSWAP spectra then lead to parametric crest distributions, which can be used easily in applications.

Table of Contents:

- [Introduction](#)
- [Previous estimates of Instrumentation](#)
- [Second-order wave profiles](#)
- [Comparisons with measurements](#)
- [Comparisons with previous Parametric crest height](#)
- [Conclusions](#)
- [REFERENCES](#)
- [FIGURES](#)

Options:

- [Create Reference](#)
- [Email this Article](#)
- [Add to MyArchive](#)
- [Search AMS Glossary](#)

Search CrossRef for:

- [Articles Citing This Article](#)

Search Google Scholar for:

- [George Z. Forristall](#)

1. Introduction

Qualitatively, the sharpening of the crests of surface waves is the most obvious manifestation of nonlinearity in the ocean.

Yet a detailed quantitative description of this phenomenon accurate enough for engineering use remains elusive. The problem is to calculate the statistical distribution of crest heights given the directional spectrum of the waves and the water depth. By crest height, we mean the highest point on a wave trace between the time it crosses above mean water level and the time it crosses below mean water level, the “zero-crossing crest height.” The alternate definition of a crest as a local maxima is not useful for engineering purposes since wave records can show many small maxima between zero crossings.

To first order, the water surface can be represented as Gaussian noise with a reasonably narrow frequency band. The crest heights then have the same distribution as the envelope of the noise, which has the Rayleigh distribution

$$P(\eta_c > \eta) = \exp\left[-8\frac{\eta^2}{H_s^2}\right], \quad (1)$$

where η_c is the crest height, $H_s = 4m^{1/2}_0$ is the significant wave height, and m_0 is the variance of the wave spectrum. We use this definition of the significant wave height throughout this paper instead of its original definition as the average of the highest $\frac{1}{3}$ of the zero crossing waves since m_0 is the more fundamental measure of the energy in the spectrum, predicted by all modern wave forecasting programs. [Forristall \(1978\)](#) and many others have shown that the $H_{1/3}$ definition usually gives values about 5% lower than the definition from the variance.

Real waves show a small but easily noticed departure from a Gaussian surface. The crests are higher and sharper than expected from a summation of sinusoidal waves with random phase, and the troughs are shallower and flatter. It is easy to tell by inspection whether a wave record is right side up.

The shape of regular progressive waves can now be calculated to a very high degree of accuracy, but no complete theory for the statistics of random waves exists. [Longuet-Higgins \(1963\)](#) used a Gram-Charlier series to describe the probability density function of the surface elevation. He calculated the moments that determine the properties of the distribution from a weakly nonlinear wave theory. The major problem with the result is that the density function is sometimes negative. [Srokosz \(1998\)](#) has recently overcome this problem by forming a Pearson distribution with a specified positive value of skewness and zero kurtosis. These distributions have the possible flaw of predicting bounds on the maximum and minimum values of the surface elevation. In addition, neither the theory of Longuet-Higgins or that of Srokosz predicts the distribution of zero-crossing crest heights, which is of most interest in applications.

A theory for the second-order interactions of waves in a random directional sea has been available for some time. It is not clear how to derive a crest height distribution directly from the theory, but it is reasonably simple to simulate time series of waves that include these interactions. Sample distributions correct to second order can thus be found through analysis of long simulated records. Serious exploration of this approach has recently begun. [Jha \(1997\)](#) has performed such simulations for unidirectional waves and compared them to laboratory and field measurements. [Prevosto \(1998\)](#) extended the work to directionally spread waves. He calculated the skewness of the surface elevation and the most probable crest heights for many combinations of spectral shapes and water depths. We use essentially the same technique but extend the work by comparing the results to several sets of field measurements. In addition, we fit Weibull distributions to simulations with a wide variety of wave steepness and Ursell numbers to produce parametric versions of wave crest distributions correct to second order, which can be used very easily in applications.

We begin with a review of some of the methods that have previously been proposed for calculating wave crest heights for engineering design. The next section discusses the principles of operation of some instruments commonly used to measure waves and the problems they may have in accurately measuring crests. Then we present the equations for the second-order interactions between wave components in a random directional sea in intermediate water depth. The results of using those equations to simulate wave crests are compared to measurements and to previous methods. Simulations for a set of JONSWAP spectra then lead to parametric crest distributions. We close with conclusions and recommendations for future work.

2. Previous estimates of extreme crests

For design purposes, a crest height is often estimated by taking the height and period of the design wave and applying a high-order regular wave theory such as Stokes fifth order. Since such regular waves are often used as input to calculate forces on a structure, this method has the advantage that the crest height used to set the deck elevation is consistent with the wave used in the force calculations. It has the disadvantage of neglecting the random and directionally spread nature of the real sea.

A popular empirical crest height distribution was presented by Haring et al. (1976) and is given as

$$P(\eta_c > \eta) = \exp\left\{-\frac{1}{2}\left(\frac{\eta^2}{m_0}\right)\left[1 - 4.37\frac{\eta}{d}\left(0.57 - \frac{\eta}{d}\right)\right]\right\}. \quad (2)$$

This equation was derived by empirical fitting to 376 hours of storm wave records including measurements with Baylor wave staffs in the Gulf of Mexico and Waverider buoys in the North Sea and the Gulf of Alaska. The distribution is a function of the variance in the spectrum, m_0 , divided by water depth, d . It gives a higher probability of high crests for shallow water, as would be expected theoretically from the increased nonlinearity of shoaling waves. It does not have any dependence on wave steepness and it reduces to the Rayleigh distribution in very deep water, which cannot be strictly correct, since deep water waves are also nonlinear. [Equation \(2\)](#) is, however, significantly different from the Rayleigh distribution for large waves anywhere on the continental shelf.

It is reasonable to suppose that the nonlinear wave surface could be approximated by an amplitude-modulated Stokes waves. In deep water, the nonlinear crest amplitude from this model is

$$r = a + \frac{1}{2}ka^2, \quad (3)$$

where a is the linear wave amplitude and k is the wavenumber. D. L. Kriebel (1998 personal communication) suggests using the wavenumber associated with the frequency of the highest waves, which he estimates as $0.95/f_p$ where f_p is the peak frequency of the spectrum. This choice seems reasonable since we are trying to estimate the distribution of the highest crests.

[Tayfun \(1980\)](#) and [Huang et al. \(1986\)](#) produced crest height distributions from the Stokes model. There is some disagreement between these authors on the exact form of the resulting distribution. [Equation \(4\)](#) below is taken from the review by [Tucker \(1991\)](#):

$$P(\eta_c > \eta) = \exp\left\{-\frac{8}{R^2}[(1 + 2R\eta/H_s)^{1/2} - 1]^2\right\}, \quad (4)$$

where $R = kH_s$ is the wave steepness.

[Kriebel and Dawson \(1991\)](#) produced a version of this distribution that does not involve taking the a square root, which is given by

$$P(\eta_c > \eta) = \exp\left[-8\frac{\eta^2}{H_s^2}\right] \exp\left[8R\frac{\eta^3}{H_s^3}\right]. \quad (5)$$

If the wave steepness becomes large, the probability density function for [Eq. \(5\)](#) can become negative, and [Kriebel and Dawson \(1993\)](#) used the same assumptions to derive the slightly different formula,

$$P(\eta_c > \eta) = \exp\left[-8\frac{\eta^2}{H_s^2}\left(1 - \frac{1}{2}R\frac{\eta}{H_s}\right)^2\right]. \quad (6)$$

[Kriebel and Dawson \(1993\)](#) also extended their distribution to intermediate water depth using the depth-dependent terms from the Stokes second-order expansion. The resulting distribution is the same as [Eq. \(6\)](#) with R replaced by R^* , an effective steepness given by

$$R^* = kH_s f_2(kd), \quad (7)$$

where

$$f_2(kd) = \frac{\cosh kd(2 + \cosh 2kd)}{2 \sinh^3 kd} - \frac{1}{\sinh 2kd}. \quad (8)$$

It seems reasonable to use R_* in a shallow water version of [Eq. \(4\)](#) as well.

3. Instrumentation

Verification of crest height distributions has been hampered by the difficulty of accurately measuring wave crests in extreme sea states. Measurements from one type of sensor often disagree with those from another type, and there is no agreement on which is correct. The basic problem is the lack of any absolute standard against which the accuracy of the sensors can be judged. The notes below illustrate the problems for some of the sensors in common use. They are not meant to be exhaustive.

a. Buoys

Buoys are the most popular instruments for collecting information on wave climate. Instrument comparisons, most notably those in WADIC ([Allender et al. 1989](#)), have demonstrated that the popular models can accurately measure integral properties of the wave field. Crests measured by buoys are, however, generally smaller than those measured by other instruments.

This underestimation of crest heights is often thought to be due to the buoy partially submerging in a crest or sliding sideways away from the highest point on a high crest. These mechanisms may play a role, but even a perfect surface following buoy will underestimate wave crests. A buoy that acts as a particle on the surface will move forward in the direction of wave propagation in the crest and backward in the trough. It will therefore spend more time than a wave staff at a fixed location in the crest, and less time in the trough.

The orbital motion of the buoy distorts the shape of the wave profile, but does not by itself make the crest measurements lower. However, almost all buoys measure wave elevation through double integration of the vertical acceleration. The absolute value of the still water elevation is thus not known, and crests heights are measured from the mean of the elevation measurements. Since the buoy spends extra time in the crest, the mean water level will be slightly higher than the true still water level, and the crest height above mean water level will be slightly too small.

The motion of the buoy is a finite amplitude effect. [James \(1986\)](#), [Srokosz and Longuet-Higgins \(1986\)](#), and [Longuet-Higgins \(1986\)](#) have all considered aspects of this problem and show that to second order, the vertical displacement of the mean surface is equal to the amount that the crest is raised. Therefore, the Lagrangian motion of the buoy cancels out the second order nonlinearity of the wave crest. The details of the buoy motion are greatly complicated by its mooring line and the random nature of the real sea, and have not yet been worked out completely. Nevertheless, the main features of the argument must still be important, so accelerometer buoys cannot be considered as a real choice for measuring the distribution of wave crests.

b. Pressure transducers

Pressure transducers are useful for measuring waves at shallow water sites or on platforms where the sensor can be mounted relatively close to the sea surface. The signal must be corrected for the attenuation of the pressure fluctuations, which increases with increasing depth and increasing wavenumber. These corrections are reasonably accurate for at least the low frequency part of the wave spectrum, but it is hard to see how the results could be useful for estimating the crest distribution. If the corrections are made with first-order theory, as is usual, the resulting surface will be Gaussian. If the difficult problem of making higher-order corrections is faced, the result will only be an expression of the theory used rather than an independent check of it.

c. The Baylor wave staff

The Baylor wave staff consists of a pair of stainless steel wire ropes separated by insulators about 20 cm long. The transducer measures the natural frequency of the inductive loop made by the two wires and the sea surface, from which the length of the loop is found. The instrument is robust and relatively immune to fouling. It has been particularly popular for wave measurements from platforms in the Gulf of Mexico.

Tests have shown that it has a linearity better than 1% and that it will record changes of elevation at least as fast as 300 m s^{-1} . Our experience from calibrating Baylor staffs is that quite a firm short is necessary before the sensor responds. It thus seems unlikely that it would be affected by spray.

d. EMI laser

The EMI laser is a pulsed range finder operating in the near-infrared region. Narrow pulses of light are produced by a laser diode, and the radiation from the target is used to stop a time interval measurement. The time of travel is converted to an analog voltage proportional to the distance to the reflector. The response of the optical unit is 10 to 15 Hz, but the output is usually filtered by a 2-Hz Butterworth filter to eliminate high frequency noise. We are aware of some tests that showed that the instrument responded to artificial spray, but we do not have details of the tests.

e. Marex radar

The Marex wave radar is a ranging device derived from a radar altimeter. The radar operates in the microwave (J) band with a beamwidth of $\pm 6^\circ$. It must be positioned on a structure so that sidelobes of the beam do not reflect from members of the structure. We do not know of any tests of its response to spray.

4. Second-order wave profiles

A second-order expansion of the sea surface can capture the effects of wave steepness, water depth, and directional spreading with no approximations other than the truncation of the expansion at second order. Higher-order interactions and other effects will of course influence the distribution of real wave crests. In particular, wave breaking could be important. The effect of wave breaking on wave heights in deep water was considered by [Tayfun \(1981\)](#), and [Thornton and Guza \(1983\)](#) considered the shallow water case. The point of our investigation is, however, to see how well a straightforward application of second-order theory can match observations.

The second-order wave interactions for infinite water depth were calculated by [Longuet-Higgins \(1963\)](#), and the calculations were extended to intermediate water depths by [Sharma and Dean \(1979\)](#). We reproduce the latter result for completeness. Let the first-order water surface be given by

$$\eta = \sum_{n=1}^N a_n \cos(\mathbf{k}_n x - \sigma_n t + \epsilon_n), \quad (9)$$

where t is time; x is the position vector in the plane; σ_n , ϵ_n , and \mathbf{k}_n are, respectively, the radian frequency, phase, and vector wavenumber of Fourier wave component n ; and a_n is its amplitude. The frequencies and wavenumbers are related by the linear dispersion equation

$$\sigma_n^2 = g|\mathbf{k}_n| \tanh(|\mathbf{k}_n|d), \quad (10)$$

where g is the acceleration of gravity and d is the water depth. The second-order correction to the wave surface given by [Sharma and Dean \(1979\)](#) is then

$$\begin{aligned} \eta^{(2)} = \frac{1}{4} \sum_{i=1}^N \sum_{j=1}^N a_i a_j \{ & K^- \cos(\psi_i - \psi_j) \\ & + K^+ \cos(\psi_i + \psi_j) \}, \quad (11) \end{aligned}$$

where

$$\begin{aligned} K^- = [D_{ij}^- - (\mathbf{k}_i \cdot \mathbf{k}_j + R_i R_j)](R_i R_j)^{-1/2} \\ + (R_i + R_j) \end{aligned} \quad (12)$$

$$\begin{aligned} K^+ = [D_{ij}^+ - (\mathbf{k}_i \cdot \mathbf{k}_j - R_i R_j)](R_i R_j)^{-1/2} \\ + (R_i + R_j) \end{aligned} \quad (13)$$

$$D_{ij}^- = \frac{(\sqrt{R_i} - \sqrt{R_j})\{\sqrt{R_j}(\mathbf{k}_i^2 - R_i^2) - \sqrt{R_i}(\mathbf{k}_j^2 - R_j^2)\}}{(\sqrt{R_i} - \sqrt{R_j})^2 - k^- \tanh k^- d}$$

$$+ \frac{2(\sqrt{R_i} - \sqrt{R_j})^2(\mathbf{k}_i \cdot \mathbf{k}_j + R_i R_j)}{(\sqrt{R_i} - \sqrt{R_j})^2 - k_{ij}^- \tanh k_{ij}^- d} \quad (14)$$

$$D_{ij}^+ = \frac{2(\sqrt{R_i} + \sqrt{R_j})^2(\mathbf{k}_i \cdot \mathbf{k}_j - R_i R_j)}{(\sqrt{R_i} + \sqrt{R_j})^2 - k_{ij}^+ \tanh k_{ij}^+ d} + \frac{(\sqrt{R_i} + \sqrt{R_j})\{\sqrt{R_i}(\mathbf{k}_j^2 - R_j^2) + \sqrt{R_j}(\mathbf{k}_i^2 - R_i^2)\}}{(\sqrt{R_i} + \sqrt{R_j})^2 - k_{ij}^+ \tanh k_{ij}^+ d} \quad (15)$$

$$k_{ij}^- = |\mathbf{k}_i - \mathbf{k}_j| \quad (16)$$

$$k_{ij}^+ = |\mathbf{k}_i + \mathbf{k}_j| \quad (17)$$

$$R_i = |\mathbf{k}_i| \tanh(|\mathbf{k}_i| d) = \sigma_i^2/g \quad \text{and} \quad (18)$$

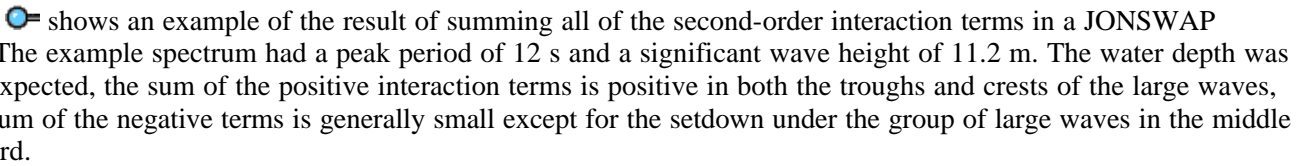
$$\psi_i = \mathbf{k}_i x - \sigma_i t + \epsilon_i \quad (19)$$

For infinite water depth, [Eq. \(7\)](#) reduces to Eq. (3.7) of [Longuet-Higgins \(1963\)](#), except that the latter equation is missing a factor of $1/2$.

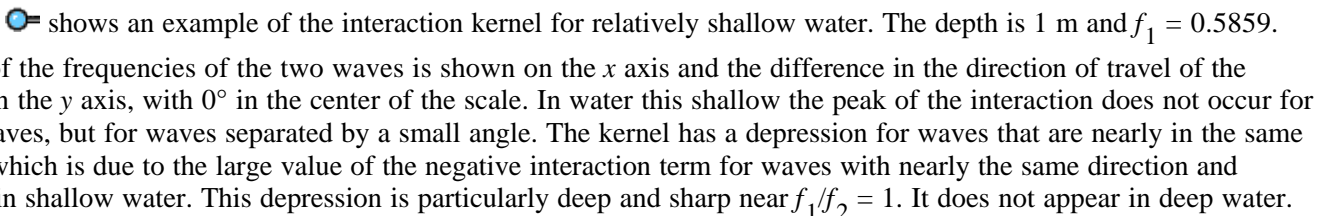
a. Form of the interaction kernel

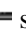
The positive interaction terms given by [Eq. \(15\)](#) occur at the sum of the frequencies of the interacting wave components. They produce the sharpening of the crests and flattening of the troughs that we associate with second-order Stokes waves. The negative interaction terms given by [Eq. \(14\)](#) occur at the difference of the frequencies of the first-order wave components. These interactions give the setdown of the water level under wave groups.

The qualitative behavior of the interactions can be understood by considering the simple case of two component waves with nearly the same frequency. For this case the positive interaction term in [Eq. \(11\)](#) has a frequency approximately twice that of the linear component waves. It will thus have positive peaks in phase with both the crests and troughs of the linear components. The frequency of the negative interaction term is the difference of the frequencies of the components, which is the beat frequency or envelope of the linear wave groups. Since the interaction kernel given by [Eq. \(12\)](#) is negative, this low frequency second-order wave will be negative under high wave groups.


[Figure 1](#) 

The skewness kernel is defined as $(K^- + K^+)/4$ and is a measure of the strength of the second-order interaction. It is a function of the frequencies of the two interacting waves as well as their angular separation and the water depth. The strength of the interaction is much greater in shallow water, matching the observation that the wave profile is more skewed in shallow water.

[Figure 2](#) 

[Figure 2](#)  shows that wave setback effects will be much more important for unidirectional waves produced in a wave tank than they are for natural waves in the ocean, which are always spread directionally to some extent.

b. Numerical implementation

The calculations indicated by [Eqs. \(11\)–\(19\)](#) are easy to implement, but represent a fair amount of computation since there are very many interactions to be calculated, particularly in the three-dimensional case. A typical simulation would have 4096 time steps at 4 Hz. A first-order simulation of a given wave spectrum is produced from [Eq. \(9\)](#) by choosing the phases ϵ_n from a uniform random distribution and calculating the wave height using an inverse fast Fourier transform to perform the summation in [eq. \(9\)](#). The second-order interactions are then calculated for each pair of component waves in the first-order simulation. The summation in [Eq. \(11\)](#) gives time series of the positive and negative interactions as shown in [Fig. 1](#) . Adding the time series of the positive and negative interactions to the first-order simulation then gives the second-order simulation.

The interactions do not have to be calculated for all of the 2048 frequencies in the Fourier transform of the time series, partly because the energy in the first-order spectrum is very small at the higher frequencies, but also because the energy in the measured spectrum at these high frequencies appears to be mostly due to nonlinear interactions. It is possible to use an iterative scheme to produce a first-order spectrum from the measured spectrum, but it is much simpler to truncate the second-order calculations at a small multiple of the peak frequency of the spectrum. This simplification has little effect on the crest height distributions. The calculations described in this paper were typically truncated for $f_1 + f_2$ greater than four or five times the peak frequency.

Repeating a simulation with precisely the same spectral variance at each Fourier line does not include all of the natural variability of waves. The variances are actually random variables with a Chi-squared distribution. If a directional spectrum is simulated, the addition of several wave components with different directions and the same frequency will automatically produce this distribution in the frequency spectrum. For consistency, we therefore multiply the input spectral lines in two-dimensional simulations by a Chi-squared random variate.

We generally want to perform many simulations using the same spectrum in order to produce stable statistics for rare crest heights. Since the skewness kernel is the same for all of the repetitions, it is efficient to calculate it once for each spectrum and store it. The calculations also exploit the fact that the kernel is symmetric in the two frequencies and depends only on the difference in the two angles. We use an angular resolution of 12° for the three-dimensional simulations.

Repeating a simulation many times with different random numbers gives enough samples to stabilize the statistics at low probability levels. In a typical example, we would use 200 repetitions of a 4096 time step simulation at 4 Hz for a spectrum with a peak period of 8 s. Running this example several times showed that the standard deviation of the crest height normalized by the significant wave height was 0.018 at a probability level of 0.001 and 0.041 at a probability level of 0.0001.


The length of the individual simulations does not have any measurable effect on the statistics, at least within the limits used in this study. To test this assertion, we did 10 000 repetitions of a unidirectional simulation with 4096 time steps and 5000 repetitions of a simulation of the same spectrum with 8192 time steps. At a probability level of 0.001, the 4096 point simulations gave a normalized crest height of 1.2256 and the 8192 point simulations gave a normalized crest height of 1.2238.

Different sample rates and numbers of repetitions were used in some of the case studies discussed below. In general, we used the same sample rate as the measurements. As discussed by [Tayfun \(1993\)](#) and shown in the Camille measurements below, the sample rate can have some effect on the statistics if there are too few sample points per fundamental wave period. Since 2D simulations are much more economical than 3D simulations, we often used many more repetitions in the 2D simulations.

5. Comparisons with measurements

a. Storms at Tern in the North Sea

The Tern platform is located in the northern North Sea between the Shetland Islands and Norway. It is about 150 km from the nearest shoreline and in 167-m water depth. It is a fairly standard eight legged steel oil production platform that was installed in 1988. It was equipped with a structural monitoring system including strain gauges, two wave height sensors, and an electromagnetic current meter. [Jonathan et al. \(1994\)](#) and [Jonathan and Taylor \(1995\)](#) give descriptions of the measurement system and the oceanographic conditions in the storms considered here.

[Figure 3](#)  shows an outline plan of the platform with the sensor locations marked. The rectangles in the figure show the

outline of the structural members of the platform at sea level (MSL), at the 41-m depth of the Marsh McBirney electromagnetic current meter, and at the mud line. A Marex wave radar was mounted under the southeast corner of the platform deck and an EMI laser wave sensor was mounted under the deck on the southwest corner. Both of these sensors measure the distance from the instrument to the instantaneous water surface.

Three storms at Tern have been studied in detail. One of the storms occurred in January 1992 and two in January 1993. The storm on 4 January 1993 is referred to as 93a and the one on 17 January 1993 is referred to as 93b. Conditions in all three storms were extreme, with peak significant wave heights above 12 m. Storms 93a and 93b are particularly useful for wave process studies since the conditions remained stationary, nearly within the limits of sampling variability, for 8 or 9 hours. Storm 92 built quickly to a peak H_s of 13.8 m and then declined.

Figures 4 and 5 show the probability distributions of the wave crest heights for storms 93a and 92 respectively. The crest heights are normalized by the significant wave height during the hour the crest was measured. If the waves were linear so that the surface elevation had a Gaussian distribution, the crest heights between zero crossings would have a Rayleigh distribution. This theoretical distribution is shown by the solid line in the figures. As expected, the sample distributions from the measurements show an excess of high crest heights above the Rayleigh curve.

The sample distributions also show a significant disagreement between the results from the two wave sensors. In storm 93a, the crests measured by the Marex radar are about 10% higher than the crests expected from linear theory, but the highest crests from the EMI laser measurements are 20%–30% higher than linear theory. In storm 92, however, the situation is reversed. The measurements from the EMI laser are about 10% above the linear curve while those from the Marex radar are much higher. It seems quite likely that the difference between the storms can be explained by the difference in wave directions, as shown in Fig. 3. In storm 93a, the waves were propagating to the north, so that their crests passed the Marex radar before encountering any structural elements on the platform. On the other hand, the leg on the southwest corner of the platform is upwave from the EMI sensor, and it is quite likely that spray caused by a wave crest hitting that leg would sometimes pass under the EMI laser. The response of wave sensors in the presence of spray is not known with any certainty, but it is reasonable to suppose that spray from structural interference could cause a laser gauge to record higher crests than those in the ambient waves.

This hypothesis is supported by the fact that in storm 92 the waves were propagating to the east so that the EMI laser was on the windward side of the platform while the Marex radar was in the lee of structural members. Apparently, both of the sensors measured crests higher than the ambient waves due to spray from structural members, although there is no obvious evidence of spray in the measured time series. The location of a wave sensor with respect to the platform it is mounted on thus may be at least as important as the response characteristics of the sensor itself.

Given the likely platform interference, we compare the second-order simulations with the Marex measurements during storm 93a and the EMI measurements during storm 92. Figure 6 shows the comparison for 93a. The ordinate in this figure gives the ratio of the crest height to the height predicted by the Rayleigh distribution at the probability level of the abscissa. It thus shows that the measured wave crests were about 10% higher than expected from linear theory and that the ratio increases slightly at lower probability levels. The measurements are for 9 hours of the storm, which included about 3000 crests.

The simulations were based on spectra calculated from the measurements for each hour. For the two-dimensional simulations, 200 repetitions for each of the nine spectra were made. The simulations were made at a 5.12-Hz sample rate, the same as the measurements, and each simulation was 4096 points long. There were therefore about 44 hours of simulation for each hour of measurements, so the statistics of the simulations are much more stable than those of the measurements. The three-dimensional simulations were based on directional spectra calculated from the wave radar and the electromagnetic current meter. Since the three-dimensional simulations demand much more computer time, only 30 repetitions were made for each spectrum, giving 6.67 hours of simulation for each hour of measurement.

The statistics of the simulations are very similar to those of the measurements, about 10% higher than linear theory and increasing slightly at lower probability levels. The three-dimensional simulations are about 2% lower than the two-dimensional simulations. The difference is caused by the slightly lower values of the second-order interaction kernel for waves that are not colinear. The two-dimensional simulations appear to be slightly higher than the measurements while the three-dimensional simulations appear to be slightly lower.

Figure 7 shows the measured and simulated statistics for storm 92. Both the measurements and the simulations are for 8 hours at the peak of the storm when the significant wave height ranged from 7.85 to 13.78 m. The 2D and 3D simulations are very similar to those for storm 93a, but the data points in the top 10% of the crests are consistently higher than the simulations. There is no obvious difference in the spectra of the two storms that would explain the difference in their crest statistics. It is possible that the response of the EMI and Marex sensors is slightly different, even when they have good exposure to the ambient waves.

b. Hurricane Opal

This storm entered the Bay of Campeche in the Gulf of Mexico on 30 September 1995 as a tropical depression. It intensified rapidly as it accelerated north–northwestward on 3 and 4 October on its way to a landfall in the panhandle of Florida. Its maximum intensity was observed early on 4 October as the eye passed 27.3°N, 88.5°W with a 916-mb central pressure and a very small eye 10 n mi in diameter.

Waves from Hurricane Opal were measured at the Bullwinkle oil production platform located at 27.9°N, 90.9°W in 410 m of water. A comprehensive instrumentation system was installed on Bullwinkle in order to measure the environment and the response of the structure. [Swanson and Baxter \(1989\)](#) give a good description of this system. A Baylor wave staff was used to measure wave elevations and three Marsh–McBirney electromagnetic current meters measured the wave particle velocities.

Since the eye of the tight storm passed 125 miles to the east of Bullwinkle, the waves there were never extremely high. We used the 14 hours of measurements from 0500 to 1800 UTC 4 October 1995 in our analysis, and the significant wave height during that time ranged from 4.78 to 6.14 m. The measurements were recorded at 4 Hz. [Figure 8](#) show the observed and simulated distributions of crest heights for Hurricane Opal. The simulations are about 2.5% lower than the simulations for the Tern storms since the waves were not as steep. The three-dimensional simulations produce crests about 1% smaller than the two-dimensional simulations, but they are still 2% larger than the bulk of the observations.

c. Hurricane Camille

Camille, whose path crossed the north-central Gulf of Mexico, was one of the most intense and destructive storms to strike the United States this century. Waves were recorded by a Baylor wave staff at station 1 of the ODGP ([Hamilton 1976](#)), which was on the South Pass 62A oil production platform located at 29°04'50"N, 88°44'30"W. Camille passed almost directly over the station, and the large waves that were measured had a great influence on setting the standard criteria for platform design in the gulf. The measurements were recorded on an analog tape recorder and, unfortunately, were only digitized at a 1-Hz sampling rate. The wave staff broke at 1630 CDT 17 August 1969, which hindcasting studies show to be very close to the peak of the storm.

Measurements and simulations of the crest heights from 1200 to 1630 CDT are shown in [Fig. 9](#). The significant wave height grew from 9.96 to 13.40 m during this period. Only two-dimensional simulations are shown since directional spectra were not measured during the storm. The simulations made at a 1-second time step agree reasonably well with the measurements, although there appears to be considerable scatter in the measurements which cause the distribution to deviate from a smooth curve. We also made simulations with a ¼-second time step, and they are significantly different, about 2.5%–3% higher. The difference is not due to the energy content of the sea at frequencies above 1 Hz, which is very small, but to the fact that 1-Hz sampling frequency is likely to miss the very peak of the waves. This effect was investigated in some detail by [Tayfun \(1993\)](#), who found that the higher waves would be underestimated by approximately $(\pi^2/6)(\Delta/\bar{T})^2$ where Δ is the sampling interval and \bar{T} is the average wave period. For the 10-s average wave periods in this part of Camille, the formula gives an error of 1.6%, close to the difference in the simulations. The relatively long sampling interval in the digitized record of the Camille waves clearly causes an underestimate of the true crest heights.

d. Shallow water waves in Lake Ontario

The Canada Centre for Inland Waters maintains a research tower at the western end of Lake Ontario near Toronto. Many interesting studies of wave processes have been conducted there, including the definitive measurements of directional spectra by [Donelan et al. \(1985\)](#). The tower is in 12 m of water. An easterly storm on 10 January 1977 produced waves that reached a significant height of 3 m at the tower. During that storm, 14 wave staffs on the tower and extensions from it were operational, and we have examined measurements from them during one hour at the peak of the storm. The measurements were recorded at 5 Hz.

Despite that the structure appears to be very transparent, a few unusually high crests were observed in the lee of the platform but not by the wave staffs on the windward side of the platform. Therefore in [Fig. 10](#) we only included data from the 6 wave staffs with the clearest upwind exposure. The two-dimensional simulation agrees very well with the measurements, while the three-dimensional simulation appears to be a bit high, at least at low probabilities. In shallow water, waves with a narrow directional spreading can be more nonlinear than unidirectional waves because the interaction kernel reaches its maximum for wave components slightly separated in direction, as shown in [Fig. 2](#).

[Figure 10](#) also shows the results of a two-dimensional simulation made with the water depth increased to 1000 m, labelled “Deep Water.” The crests in this simulation are about 3% lower than those for the true water depth of 12 m, showing the increased nonlinearity of the waves due to the shallow water at the tower.

6. Comparisons with previous estimates

Figures 11 and 12 compare our two-dimensional, second-order wave simulations with previous methods of estimating crest heights. Figure 11 is for conditions during the peak of storm 93a at Tern, for $D = 167$ m, $T_p = 14.3$ s, $H_s = 12.0$ m. Using $T_s = 0.95T_p$, we have $T_s = 13.6$ s for use in Eq. (6). The steepness, $R = 0.2628$, and the effective shallow water steepness R^* are virtually identical for this relatively deep water.

Our two-dimensional second-order simulation is shown as the solid line in the figure. The Kriebel and Dawson (1993) distribution from Eq. (6) agrees quite well with this simulation. The results from Eq. (4), labelled “Tayfun” in the figure, are a few percent lower. For the steepness of 0.2628, there is a noticeable difference between these two versions of the distribution derived from modulated Stokes waves. The distribution of Haring et al. (1976) is even lower because the water depth at Tern is deep enough that the nonlinear adjustment in Eq. (2) is too small. We also tested Eq. (2) for the 410-m water depth at Bullwinkle, and the resulting distribution (not shown) was very close to the Rayleigh distribution.

Crest heights calculated from Stokes fifth-order waves are shown as small circles in Fig. 11. The wave heights at several probabilities of exceedence were calculated from the Rayleigh distribution and the crest height of a Stokes fifth wave with that height and a period of 13.6 s was found. These crests are slightly lower than those from the second-order simulations and agree very closely with the distribution from modulated Stokes waves given by Eq. (4). The steps in this calculation of crest heights from regular waves are standard practice, but they are somewhat inconsistent since actual trough to crest wave heights are lower than given by the Rayleigh distribution. If an empirical distribution such as the one due to Forristall (1978) were used to estimate the wave heights, the Stokes crest heights for this example would be about the same as given directly by a Rayleigh distribution of crest heights.

Figure 12 is for conditions during the peak of the storm in Lake Ontario, for $D = 12$ m, $T_p = 8.36$ s, $T_s = 7.94$ s, and $H_s = 3.0$ m. The steepness is $R = 0.251$, and the effective shallow water steepness $R^* = 0.613$. We used the shallow water steepness in Eqs. (6) and (4). The Kriebel and Dawson (1993) shallow water distribution is unrealistically higher than any of the others, probably because the very high value of effective steepness invalidates the mathematical assumptions that were made in the derivation of the distribution by reversion of series. Equation (4), labeled “Tayfun,” gives a more reasonable result, but it too is considerably higher than the simulations (and the data).

The crest heights from individual Stokes fifth-order waves again agree with Eq. (4), and the Haring et al. (1976) distribution gives about the same result in this case, but all are considerably larger than the simulations. The Stokes crest heights may be too high because the regular wave method effectively concentrates all of the energy of the spectrum at one frequency, and the positive interaction term is largest for self interaction. The method also does not include the negative interaction which produces a set down under high wave groups. The Haring et al. distribution is too low for very deep water and too high for very shallow water. These differences should not be too surprising since the water depths in these examples are outside the range of water depths in the data from which this empirical distribution was developed.

The higher wave heights during this storm were somewhat higher than the normally recommended limit of applicability of Stokes second-order theory. However, for a wave height of 6 m and a period of 7.94 s, Stokes wave theory gives a crest height of 3.92 m while a 15th-order Chappelle numerical wave expansion gives a crest height of 4.08 m. The difference is noticeable, but small compared to the discrepancies in Fig. 12, and in the opposite direction.

7. Parametric crest height distributions from simulations

The second-order simulations appear to match a variety of measurements relatively well. Performing the simulations is, however, rather time consuming especially for directionally spread waves. For applications, it would be useful to have simple functional forms that match the results of the simulations. In order to produce such parametric distributions, we simulated crests for a variety of wave steepness and Ursell numbers. The spectra were constructed using the equations of Goda (1985), which give spectra similar to the JONSWAP form but with a specified peak period and significant wave height. The spectra had peak periods of 8, 10, and 12 s. The steepness based on the peak period T_p ,

$$S_p = \frac{2\pi H_s}{g T_p^2}, \quad (20)$$

varied from 0.01 to 0.10 in steps of 0.01. Most of the simulations were made using the standard JONSWAP peak enhancement factor $\gamma = 3.3$, but some simulations were also made with $\gamma = 1.0$ and 10.0. The runs were repeated for water depths of 10, 20, and 40 m and for infinite water depth. Combinations of steepness and water depth that gave physically impossible wave heights were not simulated. The three-dimensional simulations used a \cos^{2s} spreading function with the

parameter s taken from the fetch-limited measurements of [Ewans \(1998\)](#).

Each case of the two-dimensional simulations included 10 000 repetitions of a 1024-s time series at 4 Hz for statistical stability. The three-dimensional simulations require much more computer time, so only 250 repetitions were done for each case. In addition, only about half of the two-dimensional cases were included in the directionally spread simulations.

[Figure 13](#) shows some example results from the simulations in a water depth of 20 m. The simulations are for a standard JONSWAP spectrum with a peak period of 10 s. Four sets of simulations are shown with $T_p = 0.01, 0.03, 0.05,$ and 0.07 , starting from the lowest set of curves. The directionally spread simulations show more sampling variability than the unidirectional simulations since they include fewer data points. For steep waves in this water depth, the directionally spread crests are higher at low probability levels than the unidirectional crests. As mentioned before, this effect is due to the smaller low frequency setdown terms in the directionally spread waves.

The parameterization of the simulations involved two steps of fitting. First, the simulations for each case were fit to a Weibull distribution of the form:

$$P(\eta_c > \eta) = \exp\left[-\left(\frac{\eta}{\alpha H_s}\right)^\beta\right]. \quad (21)$$

Then simple expressions for the Weibull parameters α and β were found as functions of the water depth and wave spectrum. These expressions are based on parameters that characterize the degree of nonlinearity of the waves, that is, the wave steepness and Ursell number. We found that basing the wave steepness on the mean wave period, rather than the peak period, produced good fits for spectra with the same peak period but different peak enhancement factors. The steepness parameter used in the fits is thus

$$S_1 = \frac{2\pi H_s}{g T_1^2}, \quad (22)$$

where T_1 is the mean wave period calculated from the ratio of the first two moments of the wave spectrum, m_0/m_1 .

The standard parameter for characterizing the effect of water depth on the nonlinearity of waves is the Ursell number. The Ursell number based on the significant wave height and mean period is

$$Ur = \frac{H_s}{k_1^2 d^3}, \quad (23)$$

where k_1 is the wavenumber for a frequency of $1/T_1$. Proposals have been made for nonlinearity parameters which combine the effects of steepness and water depth, but we found that the fits were better when the two were included separately.

The fits are forced to match the Rayleigh distribution with $\alpha = 1/(8)^{1/2}$ and $\beta = 2$ at zero steepness and Ursell number. The fits to the two-dimensional simulations are then

$$\alpha_2 = 0.3536 + 0.2892S_1 + 0.1060Ur \quad (24)$$

$$\beta_2 = 2 - 2.1597S_1 + 0.0968Ur^2 \quad (25)$$

and the fits to the three dimensional simulations are

$$\alpha_3 = 0.3536 + 0.2568S_1 + 0.0800Ur \quad (26)$$

$$\beta_3 = 2 - 1.7912S_1 - 0.5302Ur + 0.284Ur^2. \quad (27)$$

Examples of these fits to the three-dimensional simulations are shown as the dashed lines in [Fig. 13](#). From the bottom distribution up, $S_1 = 0.0143, 0.0431, 0.0718,$ and 0.1005 . The Ursell numbers are $0.0441, 0.1322, 0.2204,$ and 0.3085 .

One of the more interesting features of the simulations is the influence of directional spreading on the crest height. [Figure 14](#) shows the ratio between the crest heights at the 1/11000 probability level for spread waves and the crest heights for unidirectional waves as determined from the fits in [Eqs. \(24\)–\(27\)](#). The ratios are shown as contour lines as a function of wave steepness, S_1 , and Ursell number. For deep water waves with $Ur \approx 0$, the unidirectional crests are slightly bigger, but in shallow water the crests in directionally spread waves are always larger. As mentioned before, this behavior is due to the much smaller setdown terms in the interaction kernel for spread waves, as shown for example in [Fig. 2](#).

8. Conclusions

Second-order simulations of wave crests agree well with measurements of high wave crests made in both deep and shallow water. Three-dimensional simulations that account for the directional spreading of waves produce crests that are about 2% lower than two-dimensional simulations in deep water. Shallow water makes the simulated waves more nonlinear and the crests higher as expected. Directionally spread crests can be higher than unidirectional waves when the water is shallow enough. All of these features appear to agree with measurements, but we cannot be too definite about the accuracy of the simulations because there is still doubt about the accuracy of the measurements.

The measured height of wave crests is apparently influenced by both the type of sensor used and the location of the sensor on a platform. The two influences have been difficult to sort out because there have been few comparisons of different instruments placed near each other. To remedy this situation, the Wave Crest Sensor Intercomparison Study (WACSIS) was conducted on the Meetpost Noordwijk research platform in the North Sea through the winter of 1997/98 ([van Unen et al. 1998](#)). In that project, waves were continuously recorded using a Baylor wave staff, Marex radar, Saab radar, and EMI laser, and video recordings of the waves were made at 2 Hz during daylight hours. The measurements in this dataset should provide a good test of second-order theory.

The second-order simulations appear to have a greater range of applicability than previous methods, which have been proposed for estimating crest height distributions. Simulations of pseudo-JONSWAP spectra indicate that the crest height distribution increases almost linearly with wave steepness. A systematic investigation of simulations for various input spectra and water depths has led to parametric distributions that match the observations and are accurate enough for engineering use.

Acknowledgments

Mark Donelan provided the data from Lake Ontario and Mike Vogel sent us the data from Hurricane Opal. The Tern data were provided by Peter Tromans and Paul Taylor, with whom I have had many stimulating discussions on the subject of wave statistics and dynamics. Dave Kriebel was very helpful in discussing the use of his distribution functions with me.

REFERENCES

- Allender, J., and Coauthors, 1989: The WADIC project: A comprehensive field evaluation of directional wave instrumentation. *Ocean Eng.*, **16**, 505–536..
- Donelan, M. A., J. Hamilton, and W. H. Hui, 1985: Directional spectra of wind-generated waves. *Philos. Trans. Roy. Soc. London*, **315A**, 509–562..
- Ewans, K. C., 1998: Observations of the directional spectrum of fetch-limited waves. *J. Phys. Oceanogr.*, **28**, 495–512.. [Find this article online](#)
- Forristall, G. Z., 1978: On the statistical distribution of wave heights in a storm. *J. Geophys. Res.*, **83**, 2353–2358..
- Goda, Y., 1985: *Random Sea and Design of Maritime Structures*. University of Tokyo Press, 323 pp..
- Hamilton, R. C., and E. G. Ward, 1976: Ocean Data Gathering Program: Quality and reduction of data. *J. Petrol. Technol.*, **28**, 337–344..
- Haring, R. E., A. R. Osborne, and L. P. Spencer, 1976: Extreme wave parameters based on continental shelf storm wave records. *Proc. 15th Int. Conf. on Coastal Engineering*, Honolulu, HI, 151–170..
- Huang, N. E., L. F. Bliven, S. R. Long, and C. C. Tung, 1986: An analytical model for oceanic whitecap coverage. *J. Phys. Oceanogr.*, **16**, 1597–1604.. [Find this article online](#)
- James, I. D., 1986: A note on the theoretical comparison of wave staff and wave rider buoys in steep gravity waves. *Ocean Eng.*, **13**, 209–214..

Jha, A. K., 1997: Nonlinear stochastic models for loads and responses of offshore structures and vessels. Ph.D. dissertation, Stanford University, 70 pp..

Jonathan, P., and P. H. Taylor, 1995: On irregular, nonlinear waves in a spread sea. *J. Offshore Mech. Arctic Eng.*, **119**, 37–41..

—, —, and P. S. Tromans, 1994: Storm waves in the northern North Sea. *Proc. Seventh Int. Conf. on the Behavior of Offshore Structures (BOSS)*, Boston, MA, ASCE, 481–494..

Kriebel, D. L., and T. H. Dawson, 1991: Nonlinear effects on wave groups in random seas. *J. Offshore Mech. Arctic Eng.*, **113**, 142–147..

—, and —, 1993: Nonlinearity in wave crest statistics. *Proc. Second Int. Symp. on Ocean Wave Measurement and Analysis*, New Orleans, LA, ASCE, 61–75..

Longuet-Higgins, M. S., 1963: The effect of non-linearities on statistical distributions in the theory of sea waves. *J. Fluid Mech.*, **17**, 459–480..

—, 1986: Eulerian and Lagrangian aspects of surface waves. *J. Fluid Mech.*, **173**, 683–707..

Prevosto, M., 1998: Effect of directional spreading and spectral bandwidth on the nonlinearity of the irregular waves. *Proc. Eighth Int. Offshore and Polar Engineering Conference*, Montreal, PQ, Canada, International Society of Offshore and Polar Engineers, 119–123..

Sharma, J. N., and R. G. Dean, 1979: Development and evaluation of a procedure for simulating a random directional second order sea surface and associated wave forces. Ocean Engineering Rep. 20, University of Delaware, 112 pp. [Available from Ocean Engineering Laboratory, University of Delaware, Newark, DE 19716.].

Srokosz, M. A., 1998: A new statistical distribution for the surface elevation of weakly nonlinear water waves. *J. Phys. Oceanogr.*, **28**, 149–155.. [Find this article online](#)

—, and M. S. Longuet-Higgins, 1986: On the skewness of sea surface elevation. *J. Fluid Mech.*, **164**, 487–497..

Swanson, R. C., and G. D. Baxter, 1989: The Bullwinkle platform instrumentation system. *Proc. 21st Annual Offshore Technology Conf.*, Houston, TX, Mar. Technol. Soc., 93–100..

Tayfun, M. A., 1980: Narrow-band nonlinear sea waves. *J. Geophys. Res.*, **85**, 1548–1552..

—, 1981: Breaking-limited wave heights. *J. Waterway, Ports, Coastal Ocean Eng.*, **107**, 59–69..

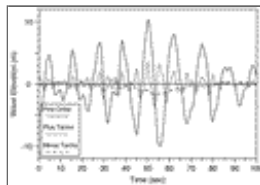
—, 1993: Sampling-rate errors in statistics of wave heights and periods. *J. Waterways, Ports, Coastal Ocean Eng.*, **119**, 172–192..

Thornton, E. B., and R. T. Guza, 1983: Transformation of wave height distribution. *J. Geophys. Res.*, **88**, 5925–5938..

Tucker, M. J., 1991: *Waves in Ocean Engineering: Measurement, Analysis, Interpretation*. Ellis Horwood, 487 pp..

van Unen, R. F., A. A. van Beuzekom, G. Z. Forristall, J.-P. Mathisen, and J. Starke, 1998: Wacsis—Wave crest sensor intercomparison study at the Meetpost Noordwijk measurement platform. *Oceans'98*, Nice, France, IEEE, 192–197..

Figures



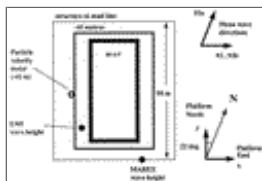
[Click on thumbnail for full-sized image.](#)

Fig. 1. An example of first- and second-order waves for a JONSWAP spectrum with a peak period of 12 s and a significant wave height of 11.2 m in 40-m water depth. The solid line shows the first-order simulation, the short dashed line shows the sum of the positive second-order terms, and the long dashed line shows the sum of the negative second-order terms.



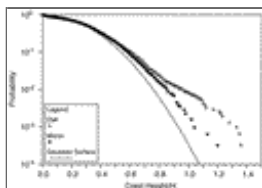
[Click on thumbnail for full-sized image.](#)

Fig. 2. Second-order interaction kernel for waves in shallow water.



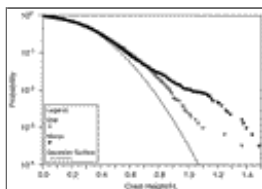
[Click on thumbnail for full-sized image.](#)

Fig. 3. Outline plan of the Tern platform with locations of the wave height sensors and the mean wave directions for the storms.



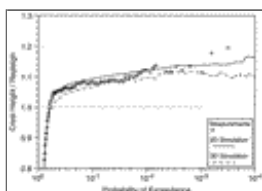
[Click on thumbnail for full-sized image.](#)

Fig. 4. Probability distribution of normalized crest heights measured at Tern during the storm on 4 Jan 1993. The crest heights are normalized by the significant wave height during each hour of the measurements. Nine hours of measurements with an average significant wave height of about 12 m were combined to produce the observed distribution.



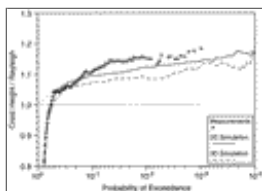
[Click on thumbnail for full-sized image.](#)

Fig. 5. Probability distribution of normalized crest heights measured at Tern during the storm on 1 Jan 1992. The crest heights are normalized by the significant wave height during each hour of the measurements. Eight hours of measurements with an average significant wave height of about 11 m were combined to produce the observed distribution.



[Click on thumbnail for full-sized image.](#)

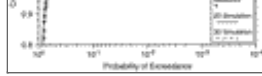
Fig. 6. Distribution of crest heights in storm 93a at Tern on 4 Jan 1993. The ordinate shows the crest height normalized by the height predicted at that probability level by the Rayleigh distribution. The measurements are from the Marex wave radar.



[Click on thumbnail for full-sized image.](#)

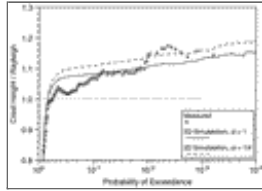
Fig. 7. Distribution of crest heights during storm 92 at Tern on 1 Jan 1992. For an explanation of the curves, see [Fig. 6](#).





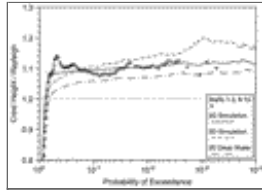
Click on thumbnail for full-sized image.

Fig. 8. Distribution of crest heights during Hurricane Opal at Bullwinkle. For an explanation of the curves, see [Fig. 6](#).



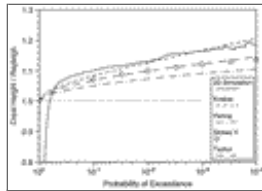
Click on thumbnail for full-sized image.

Fig. 9. Distribution of crest heights during Hurricane Camille at SP62 for 1200–1600 CDT 17 Aug 1969. For an explanation of the curves, see [Fig. 6](#).



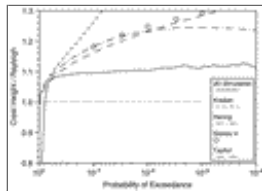
Click on thumbnail for full-sized image.

Fig. 10. Distribution of crest heights at the CCIW tower on 10 Jan 1977.



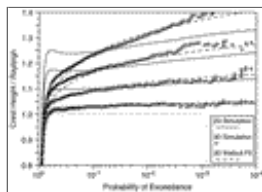
Click on thumbnail for full-sized image.

Fig. 11. Comparison of crest height distributions at Tern for $D = 167$ m, $T_s = 13.6$ s, $H_s = 12.0$ m.



Click on thumbnail for full-sized image.

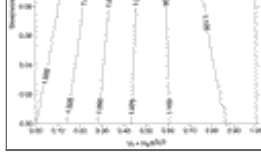
Fig. 12. Comparison of crest height distributions at the CCIW tower for $D = 12$ m, $T_s = 7.94$ s, $H_s = 3.0$ m.



Click on thumbnail for full-sized image.

Fig. 13. Normalized crest height distributions for a mean JONSWAP spectrum with a peak period of 10 s in a water depth of 20 m. Solid lines show unidirectional simulations, small circles show directionally spread simulations and dashed lines show the Weibull fits to the spread simulations. Simulations for four values of steepness are shown with $S_p = 0.01, 0.03, 0.05,$ and 0.07 starting from the bottom set of curves.





[Click on thumbnail for full-sized image.](#)

Fig. 14. The contour lines show the ratio between the crest heights of directionally spread and unidirectional waves at a probability level of 1/1000 as a function of steepness and Ursell number.

Corresponding author address: Dr. George Z. Forristall, Shell E&P Technology, Box 481, Houston, TX 77001.

E-mail: gzforristall@shellus.com

[top](#) ▲



© 2008 American Meteorological Society [Privacy Policy and Disclaimer](#)
Headquarters: 45 Beacon Street Boston, MA 02108-3693
DC Office: 1120 G Street, NW, Suite 800 Washington DC, 20005-3826
amsinfo@ametsoc.org Phone: 617-227-2425 Fax: 617-742-8718
[Allen Press, Inc.](#) assists in the online publication of *AMS* journals.